Lelai Zhou[1]
Department of Mechanical
and Manufacturing Engineering,
Aalborg University,
Aalborg 9220, Denmark
e-mail: lzh@m-tech.aau.dk

Shaoping Bai
Associate Professor
Department of Mechanical
and Manufacturing Engineering,
Aalborg University,
Aalborg 9220, Denmark
e-mail: shb@m-tech.aau.dk

A New Approach to Design of a Lightweight Anthropomorphic Arm for Service Applications

This paper describes a new approach to the design of a lightweight robotic arm for service applications. A major design objective is to achieve a lightweight robot with desired kinematic performance and compliance. This is accomplished by an integrated design optimization approach, where robot kinematics, dynamics, drive-train design and strength analysis by means of finite element analysis (FEA) are generally considered. In this approach, kinematic dimensions, structural dimensions, and the motors and the gearboxes are parameterized as design variables. Constraints are formulated on the basis of kinematic performance, dynamic requirements and structural strength limitations, whereas the main objective is to minimize the weight. The design optimization of a five degree-of-freedom (dof) lightweight arm is demonstrated and the robot development for service application is also presented. [DOI: 10.1115/1.4028292]

1 Introduction

Lightweight robots are increasingly used in service and space explorations. A service robot has to be lightweight and compliant for safe interactions with humans and for energy efficiency. For service robots, however, they have to be lightweight. This implies that a lightweight robot needs to be designed with new approach, which is able to address lightweight and structural strength, the two major design challenges.

Some attempts in making lightweight designs can be found in literature. A notable example is the DLR robotic arm [1] developed for robotic interaction in human environment. Chedmail and Gautier [2] proposed a method for the optimum selection of robot actuators to minimize the total mass of all the actuators. A robotic manipulator with hybrid actuation combining air muscles and DC motor were developed on the base of distributed macromini actuation approach [3]. Design optimization was conducted on the drive-train of two joints from an industrial manipulator [4]. MODELICA, a simulation software with robotic optimization facilities, could tune the parameters of a controller by a multicriteria parameter optimization method to improve the system dynamics [5]. A drive-train design optimization approach was presented in Ref. [6], which can minimize the weight of the robot and simultaneously select the optimal components of the drive-train.

A lightweight design may end up with a robot that is too "soft," which makes the system prone to undesirable vibrations. Design constraints on compliance thus need to be considered. To this end, FEA can be used. However, the FEA was rarely used in robotic arm design and structural optimization [7–9].

In the meantime, kinematics is also an important issue to be considered for improvement of robotic performance, either kinematic or dynamic one. An integrated structure–control design optimization method of a two-link flexible robot arm was presented, where the structural and control parameters were optimized simultaneously [10]. Evolutionary optimization method was used to optimize the parameters of a manipulator in Ref. [11]. Optimal dynamic performance based methods was reported in Ref. [12], among others. It can be noticed that structural dimensions of robotic manipulators were rarely considered. Moreover, dimensional and drive-train optimizations were mostly conducted separately. An integrated approach is desired, which allows to account for the influences of the dimensional variables and drive-train parameters in robot design, while reducing the weight through optimization.

In this work, a design method is developed for the lightweight robotic manipulators. The method combines the kinematics, dynamics, and structural strength analysis in a single design stage, while the main objective is to minimize the weight of the robot. The proposed method extends the integrated design optimization method reported in authors' previous work [13]. In the new method, the structural dimensions of a robotic arm are taken as variables in the design optimization, in addition to the parameters of the drive-trains. The arm structure and the drive-train will be optimized to obtain lightweight robotic arm with constraints on the kinematics, drive-train dynamics, and structural strength. The paper shows that the integrated optimization method can contribute to further reducing the arm weight. The system development and prototype of the robotic arm is described, with the electronics and control strategy being presented.

2 A Robotic Arm Design Model

The lightweight robotic arm considered in this paper has 5 dof, with 2 dof at the shoulder, one at the elbow, and two at the wrist, as shown in Fig. 1. This is a humanlike arm design, which can be mounted on an electric wheelchair to assist disabled in simple manipulations like picking, placing, door opening, etc., or mounted on a foundation for food feeding and drink serving.

2.1 Design Considerations. The conceptual design of the 5 dof robotic arm was developed for daily activity assistance. The total reach distance of the robot is 1 m (without the gripper), which is a bit longer than a human arm. The workspace (WS) of each joint is based on the corresponding joint WS of the human arm. The range of each joint WS is listed in Table 1.

The 5dof robotic arm designed in this work adopts a modular approach. Harmonic Drive™ CPU series gearboxes are used as transmission elements and, simultaneously, as the mechanical joints for different dof. To increase the torque capabilities of joints

[1]Corresponding author.

Contributed by the Mechanisms and Robotics Committee of ASME for publication in the JOURNAL OF MECHANISMS AND ROBOTICS. Manuscript received June 14, 2012; final manuscript received August 1, 2014; published online December 4, 2014. Assoc. Editor: Xianmin Zhang.

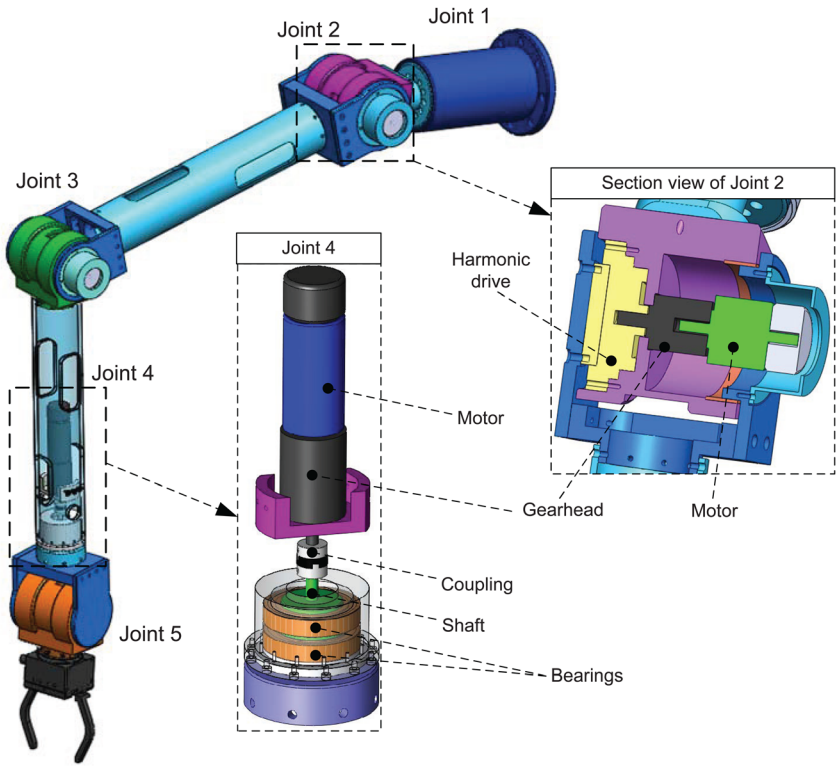

Fig. 1 Conceptual design of a 5 dof lightweight anthropomorphic arm

1, 2, and 3, a second stage of gearhead is used between Harmonic Drive and the motor. Joints 2, 3, and 5 adopt the similar configurations. In joint 4, only geared motor is used to transmit torque through bearing supported shaft, as shown in Fig. 1. The gripper, selected from SOMMER™ Automatic, is controlled by its customized controller.

2.2 Robot Modeling. The lightweight robotic arm is a serial manipulator consisting of several links connected in series by revolute joints. The kinematic and dynamic modeling was described in Ref. [13]. We introduce briefly these models for completeness.

2.2.1 Kinematics. The kinematics is formulated based on Denavit–Hartenberg's convention [14]. Cartesian coordinate systems are attached to each link of a manipulator, as shown in Fig. 2. The corresponding D–H parameters can be obtained as listed in Table 2.

The joint angular velocity can be calculated with the Jacobian matrix

$$\dot{\boldsymbol{\theta}} = \mathbf{J}^{-1}\mathbf{v}_{\text{ef}} \tag{1}$$

where $\dot{\boldsymbol{\theta}} = [\dot{\theta}_1, \dot{\theta}_2, \ldots, \dot{\theta}_n]^{\text{T}}$ is an n-dimensional (n denotes the number of dof) vector of the joint angular velocities, $\mathbf{J}$ the Jacobian matrix, and $\mathbf{v}_{\text{ef}}$ the velocity of the end-effector.

As the robot has 5 dof, its Jacobian is a nonsquare matrix. The inverse Jacobian can be found with a method reported in Ref. [15]. When the desired end-effector velocity $\mathbf{v}_{\text{ef}}$ is given, the joint angular velocity can be solved by Eq. (1).

Table 1 Joint WS of the robotic arm

Joint i	Max WS	Constrained WS
1	$0 \sim 2\pi$	$0 \sim \pi$
2	$0 \sim 3\pi/2$	$0 \sim 3\pi/2$
3	$0 \sim 3\pi/2$	$0 \sim 3\pi/4$
4	$0 \sim 2\pi$	$0 \sim 2\pi$
5	$0 \sim 3\pi/2$	$0 \sim 3\pi/4$

2.2.2 Inverse Dynamics. The integrated structural and drive-train optimization utilizes a dynamic model of the robotic arm for dynamic evaluations. The governing equation of the arm motion can be written as

$$\mathbf{M}(\boldsymbol{\theta})\ddot{\boldsymbol{\theta}} + \mathbf{v}(\boldsymbol{\theta}, \dot{\boldsymbol{\theta}}) + \mathbf{g}(\boldsymbol{\theta}) = \boldsymbol{\tau} \tag{2}$$

where $\mathbf{M}$ is the mass matrix, $\mathbf{v}$ is the vector of Coriolis and centrifugal terms of the links, $\mathbf{g}$ is the vector of gravitational forces, and $\boldsymbol{\tau}$ is the vector of joint torques. The mass matrix $\mathbf{M}$ of Eq. (2) is not constant. Instead, it changes with arm poses, arm dimensions, and mass distributions.

3 An Integrated Design

The design problem in this work is formulated as an optimization problem with an objective to minimize the weight of the robotic arm with constraints on kinematics performance,

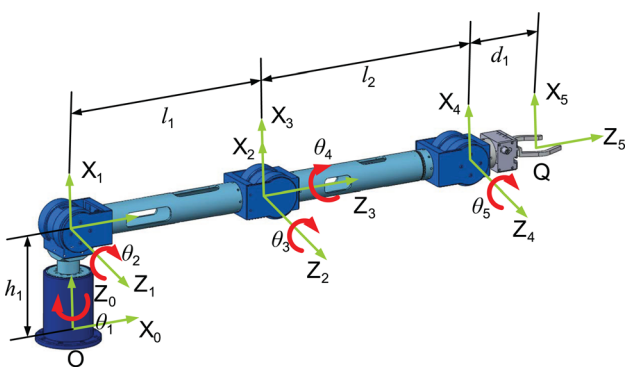

Fig. 2 Robotic arm coordinate system

Table 2 D–H parameters of the robotic arm

Joint i	α_i	a_i	d_i	θ_i
1	$\pi/2$	0	h_1	θ_1
2	0	l_1	0	θ_2
3	$\pi/2$	0	0	θ_3
4	$-\pi/2$	0	l_2	θ_4
5	$\pi/2$	0	d_1	θ_5

drive-train, and the structural strength. The selection of a drive-train is constrained through the dynamic equation and the design criteria for motors and gearboxes. The structural dimensions influence the robotic dynamics. On the other hand, they also determine the kinematic performance of the robotic manipulator. This may be formulated as a constraint on the kinematic performance index as described presently.

3.1 Parameterized Dimensions. The structural parts of the robotic arm are to be optimized in the integrated optimization method. Figure 3 shows some parameterized dimensions of the robotic arm. These dimensions fall into two groups: the assembling dimensions including the link lengths of the upper arm l_1 and the lower arm l_2, and the structural dimensions displayed in Fig. 3(*b*). The assembling dimensions determine the robotic arm's kinematic performance, while the structural dimensions affect the arm structural strength. The descriptions of the parameterized dimensions are listed in Table 3.

In this design, the inner radius r_a and r_b are taken as design variables, as well as the widths of the opening slots w_{h1} and w_{h2}. The outer radius R_a and R_b are kept constant. The dimensions a_1, a_2, b_1, and b_2, which are used to position the slots, are fixed. Other dependent dimensions are calculated accordingly: $l_{s1} = l_1 - 150$ (mm), $l_{s2} = l_2 - 150$ (mm), $l_{h1} = (l_{s1} - a_1 - a_2 - 30)/2$ (mm), $l_{h3} = l_{h2}/2$ (mm), $l_{h2} = 2(l_{s2} - b_1 - b_2 - 30)/3$ (mm).

Table 3 Structural parameters of the robotic arm (mm)

Upper arm	Lower arm	Parameter descriptions	Note
l_{s1}	l_{s2}	Tube length	Dependent variable
r_a	r_b	Inner radius	Design variable
R_a	R_b	Outer radius	Fixed
w_{h1}	w_{h2}	Widths of the opening slots	Design variable
l_{h1}	l_{h2}, l_{h3}	Lengths of the opening slots	Dependent variable
a_1, a_2	b_1, b_2	Lengths used to position the slots	Fixed

All the dimensional variables are classified into two groups, kinematic dimensions $\mathbf{u}_k = [l_1, l_2]$ and structural dimensions $\mathbf{u}_s = [r_a, r_b, w_{h1}, w_{h2}]$. The design variables are hence defined in a vector $\mathbf{u}_d = [\mathbf{u}_k, \mathbf{u}_s]$.

3.2 Constraint of Kinematic Performance. The integrated optimization is proposed to minimize the weight of the robotic arm with constraints on kinematics performance, drive-train, and the structural strength. The selection of a drive-train is constrained through the dynamic equation and the selecting criteria for motors and gearboxes. The structural dimensions influence the robotic dynamics. On the other hand, they also determine the kinematic performance of the robotic manipulator. This may be formulated as a constraint on the kinematic performance index as described presently.

The kinematics performance is one of the major concerns in robot design. It is desirable for a robot to have a high kinematics performance, while the drive-train is optimized. Several performance indices are available for the design of robotic manipulators.

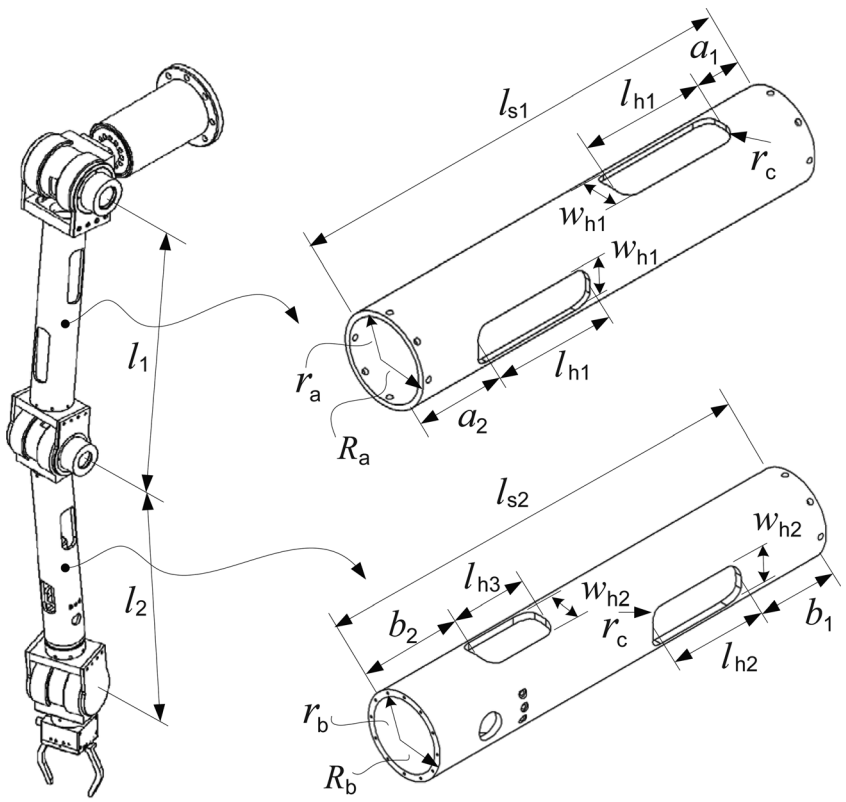

Fig. 3 Dimensional parameters of the robotic arm

They include manipulability measure proposed by Yoshikawa [16] and the global conditioning index (GCI) by Gosselin and Angeles [17]. The GCI, which describes the isotropy of the kinematic performance, is considered in this work.

The GCI within a WS W is defined as

$$\mathrm{GCI} = \frac{\int_W \frac{1}{\kappa} \mathrm{d}W}{\int_W \mathrm{d}W} \tag{3}$$

with the condition number κ given by

$$\kappa = \|\mathbf{J}(\boldsymbol{\theta}, \mathbf{u}_k)\| \left\|\mathbf{J}^{-1}(\boldsymbol{\theta}, \mathbf{u}_k)\right\| \tag{4}$$

where $\mathbf{J}(\boldsymbol{\theta}, \mathbf{u}_k)$ is the Jacobian matrix and $\boldsymbol{\theta}$ is the vector of joint angles.

In practice, the GCI of a robotic manipulator is calculated through a discrete approach as [18]

$$\mathrm{GCI} = \frac{1}{V} \sum_{i=1}^{m} \frac{1}{\kappa_i} \Delta V_i \tag{5}$$

where V is the WS volume, and m is the number of discrete points. In the case of equal-volumetric discretization, $\Delta V_i \equiv \Delta V$, Eq. (5) is transformed to

$$\mathrm{GCI} = \frac{1}{m} \sum_{i=1}^{m} \frac{1}{\kappa_i} \tag{6}$$

To keep a high kinematics performance with selected link lengths in the integrated optimization, a constraint is given on the GCI

$$\mathrm{GCI}(\mathbf{u}_k) \geq C_{\min} \tag{7}$$

where $C_{\min}$ is the minimum acceptable GCI.

3.3 Drive-Train Constraints. A drive-train model of a single joint is shown in Fig. 4. The drive-train consists of a motor, a linkage, and a gearbox for speed reduction. Taking into account of gear efficiency, the required motor torque for the ith joint can be calculated by

$$\tau_{m,i} = \left\{ (J_m + J_g)\ddot{\theta}(t)\rho + \frac{\tau(t)}{\rho \eta_g} \right\}_i; \quad i = 1, \ldots, 5 \tag{8}$$

where ρ_i is the gear ratio. $J_{m,i}$ is mass moment of inertia of the ith motor; $J_{g,i}$ is the equivalent mass moment of inertia of the ith gearbox reflected at the motor shaft; $\eta_{g,i}$ is the corresponding gear efficiency; and $\tau_i(t)$ is the load at the output link, which can be solved by Eq. (2).

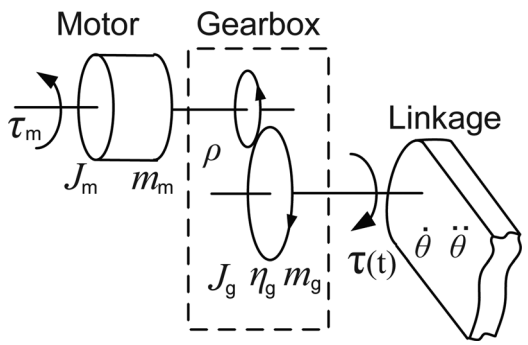

Fig. 4 Schematic view of drive-train model for a single joint

3.3.1 Motor Selection Criteria. Motors for robotic arms are usually selected from two motor groups, brushed and brushless DC motors. In selecting motors, the following three criteria are considered:

$$\tau_{\mathrm{rms}} \leq T_m; \quad \tau_p \leq T_m^{\max}; \quad n_p \leq N_m^{\max} \tag{9}$$

where τ_{rms} denotes the root mean square (RMS) value of the required motor torque, and T_{m} is the nominal torque of the motor. $\tau_p = \max\{|\tau_{\mathrm{m}}|\}$ is the required peak torque, and $T_{\mathrm{m}}^{\max}$ is the stall torque of the motor. $n_p = \max\{|2\pi\dot{\theta}(t) \cdot \rho|\}$ is the required peak speed corresponding to the motor, and $N_{\mathrm{m}}^{\max}$ denotes the maximum permissible speed of the motor.

3.3.2 Gearbox Selection Criteria. For the selection of gearboxes, the following three criteria apply. The first criterion is the root mean cubic (RMC) value of torques (τ_{rmc}), recommended by the Harmonic Drive gearbox manufacturer [19]. The RMC value is a measure of the accumulated fatigue on a structural component and reflects typical endurance curves of steel and aluminum [20]. It is therefore relevant to gearbox lifetime, and this criterion has also been used in robotic applications [21]. Other criteria include maximum output torque and input speed. The criteria are expressed as

$$\tau_{\mathrm{rmc}} \leq T_g; \quad \tau_g \leq T_g^{\max}; \quad n_g \leq N_g^{\max} \tag{10}$$

where $\tau_{\mathrm{rmc}} = \sqrt[3]{1/\Delta t \int_0^{\Delta t} \tau^3(t) dt}$, with $\tau(t)$ being the required torque from the gearbox output. T_g is the limit for rated torque of the gearbox. $\tau_g = \max\{|\tau(t)|\}$ denotes the required peak torque with respect to the output side, and $T_g^{\max}$ is the allowable peak torque of the gearbox. $n_g = \max\{|\dot{\theta}(t) \cdot \rho|\}$ is the required maximum input peak speed, and $N_g^{\max}$ denotes the maximum permissible input speed of a gearbox.

3.4 Structural Strength Constraints. While the robotic arm becomes lighter, its stiffness also reduces. To prevent the robot becoming too "soft," constraints on structural strength can be included in optimization. In this work, the stress and deformation of the robotic arm are considered. To maintain the strength and stiffness of the structure, the maximum von-Mises stress has to be smaller than the yield strength of the material

$$S_{\max} < S_y \tag{11}$$

The maximum deformation of the end-effector has to be under a relevant limit for operational consideration of the robot.

$$D_{\max} < D_{\lim} \tag{12}$$

In some cases, upper limits may be applied to the arm to make sure the structure has an acceptable compliance for safety.

3.5 Objective Function. The objective of the integrated design optimization is to design a lightweight robotic arm. The task is to find the lightest combination of motor and gearbox for all five joints and the optimal link lengths that fulfill all constraints associated with the kinematic, strength, and drive-train constraints. The optimization will also minimize the mass of the robotic structure (m_{arm}) by selecting optimal dimensions that fulfill structural constraints. The objective function, $f(\mathbf{x})$, is defined as

$$\min_{\mathbf{x}} f(\mathbf{x}) = \sum_{i=1}^{n} \left\{ m_m(\mathbf{u}_m) + m_g(\mathbf{u}_g) \right\}_i + m_{\mathrm{arm}}(\mathbf{u}_d)$$
$$\mathbf{x} = [\mathbf{u}_m, \mathbf{u}_g, \mathbf{u}_d] \tag{13}$$

S.T.

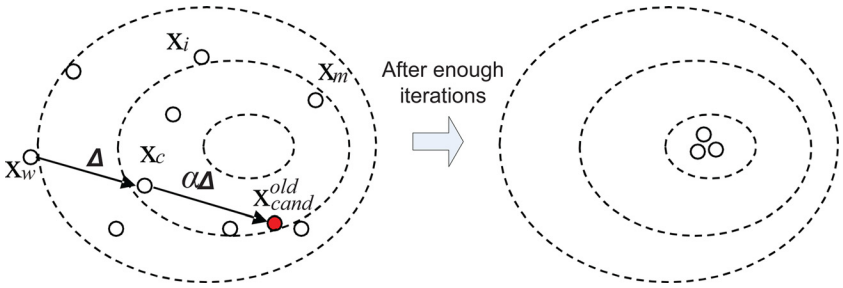

Fig. 5 Illustration of the complex method

Kinematic constraint

$$C_{\min} \le \mathrm{GCI}(\mathbf{u}_k) \tag{14a}$$

Strength constraints

$$S_y > S_{\max}(\mathbf{u}_s) \tag{14b}$$

$$D_{\lim} > D_{\max}(\mathbf{u}_s) \tag{14c}$$

Drive-train constraints

$$T_{m,i} \ge \sqrt{\frac{1}{\Delta t}\int_0^{\Delta t}\left\{\left(J_m(\mathbf{x})+J_g(\mathbf{x})\right)\ddot{\theta}(t)\rho+\frac{\tau(t,\mathbf{x})}{\rho\eta_g}\right\}_i^2\cdot \mathrm{d}t} \tag{14d}$$

$$T_{m,i}^{\max} \ge \max\left\{\left|\left(J_m(\mathbf{x})+J_g(\mathbf{x})\right)\ddot{\theta}(t)\rho+\frac{\tau(t,\mathbf{x})}{\rho\eta_g}\right|\right\}_i \tag{14e}$$

$$N_{m,i}^{\max} \ge \max\left\{\left|2\pi\dot{\theta}(t)\cdot\rho\right|\right\}_i \tag{14f}$$

$$T_{g,i} \ge \sqrt[3]{\frac{1}{\Delta t}\int_0^{\Delta t}\tau_i^3(t,\mathbf{x})\cdot \mathrm{d}t} \tag{14g}$$

$$T_{g,i}^{\max} \ge \max\{|\tau(t,\mathbf{x})|\}_i \tag{14h}$$

$$N_{g,i}^{\max} \ge \max\left\{\left|\dot{\theta}(t)\cdot\rho\right|\right\}_i \tag{14i}$$

Design variables of $\mathbf{x}$ include the index numbers of motors $\mathbf{u}_{\mathrm{m}} = [u_{m,1},\ldots,u_{m,n}]$ and gearboxes $\mathbf{u}_g = [u_{g,1},\ldots,u_{g,n}]$, relative to databases containing commercially available components, and an array of dimensional variables $\mathbf{u}_d = [\mathbf{u}_k,\mathbf{u}_s] = [l_1,l_2,r_a,r_b,w_{h1},w_{h2}]$. m_m and m_g are the mass of motors and gearboxes, respectively. So far, we have formulated the design problem as a discrete optimization problem, which can be solved by commercial available codes.

3.6 Implementation of Integrated Design. The integrated design optimization problem is solved by the Complex method, a method suitable for nonlinear and discrete optimization problems. In this section, the complex method is briefed first, followed by the procedure of optimization.

Table 4 Design space of the dimensional variables

Dimension	Range	Stepsize
r	[0.3, 0.7]	0.05
r_a	[30, 34] mm	1
r_b	[28, 31] mm	1
w_{h1}	[20, 60] mm	10
w_{h2}	[20, 60] mm	10

3.6.1 Optimization by the Complex Method. The Complex method is a nongradient based optimization method [22]. With this method, a number of points (sets of design variables) will be evaluated against the objective function. The set of design variables minimizing the objective function is denoted as the best point $\mathbf{x}_b$, while the one maximizing the objective function is denoted as the worst point $\mathbf{x}_w$. Their corresponding values of objective function are noted as the best and worst values. After each evaluation, a candidate point is generated by reflecting the worst point through the centroid $\mathbf{x}_c$ with a reflection coefficient α (as shown in Fig. 5).

$$\mathbf{x}_{\mathrm{cand}} = \mathbf{x}_c + \alpha(\mathbf{x}_c - \mathbf{x}_w) \tag{15}$$

where $\mathbf{x}_{\mathrm{c}} = 1/(m-1)\sum_{i=1}^{m}\mathbf{x}_i, \mathbf{x}_i \ne \mathbf{x}_j$. The coefficient α is experimentally determined, which takes the value of 1.3. To avoid converging at a local minimal, the candidate point can be found through a modified approach [23]

$$\mathbf{x}_{\mathrm{cand}}^{\mathrm{new}} = \frac{1}{2}\left(\mathbf{x}_{\mathrm{cand}}^{\mathrm{old}} + \varepsilon\mathbf{x}_c + (1-\varepsilon)\mathbf{x}_b\right) + (\mathbf{x}_c - \mathbf{x}_b)(1-\varepsilon)(2K-1) \tag{16}$$

where K is a random number varying in the interval [0,1]. Moreover

$$\varepsilon = \beta^{-\beta}; \quad \beta = 1 + \frac{k_{\mathrm{r}}-1}{n_{\mathrm{r}}} \tag{17}$$

Here, k_{r} is the number of repeating times the point has repeated itself, and n_{r} is a parameter, which is recommended as 4 in the program. The algorithm converges when the difference between

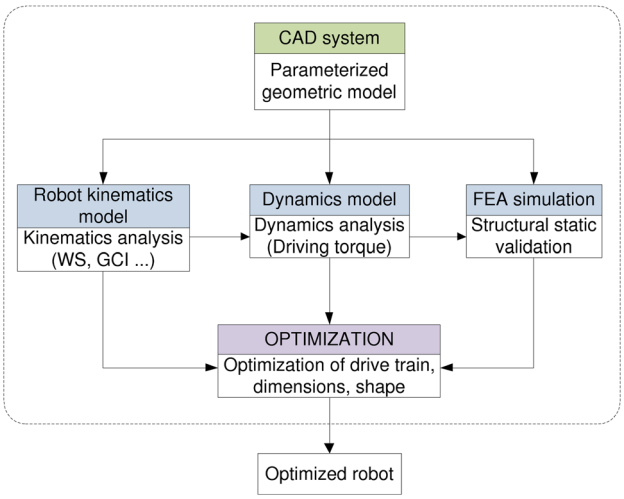

Fig. 6 Functional modules of the integrated optimization approach

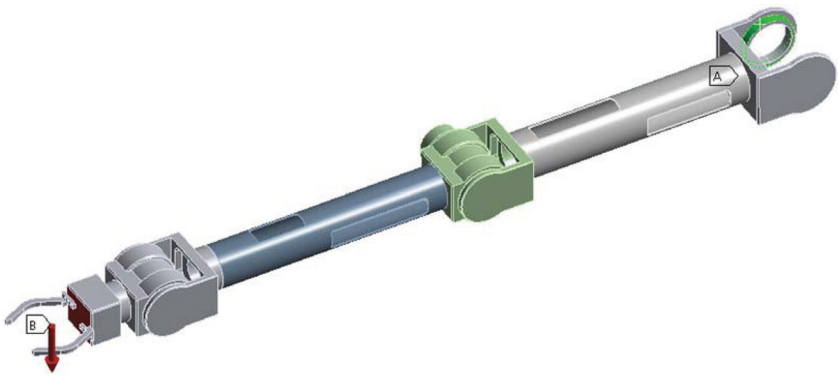

Fig. 7 Boundary conditions of the FEA model

the best and worst objective function values is less than a user defined tolerance.

3.6.2 Design Variables Programming. The design solutions yield from the Complex method is usually continuous. However, the design variables $\mathbf{u}_m$ and $\mathbf{u}_g$ have to be integers, since they are the index numbers from the databases of motors and gearboxes. To deal with the integer design variables, a round function is introduced to transfer the design variables into integers. The rounding function is given as

$$x_{\mathrm{DV}} = \mathrm{round}(x) = \begin{cases} x_{int}; & \text{if} \quad x_{int} \le x < x_{int} + 0.5 \\ x_{int} + 1; & \text{if} \quad x_{int} + 0.5 \le x < x_{int} + 1 \end{cases} \tag{18}$$

where x is the design variable manipulated by the complex method, x_{int} is the integral part of the number x, and x_{DV} is the rounded design variable. The rounded variable x_{DV} is used to update the mass of motors and gearboxes in inverse dynamic analysis, as well as the allowable torque and speed values used to examine constraint violations.

In practice, the dimensional design variables $\mathbf{u}_d = [\mathbf{u}_k, \mathbf{u}_s]$ are discretized in the design space with suitable step sizes, as provided in Table 4. To keep the reachable space of the robotic arm constant, the total reaching distance $L = l_1 + l_2$ is fixed. One nondimensional design variable r is introduced as $r = l_1/L$. Considering the structural issues, a minimum length is required for both lower and upper arms, which means $r \in [r_{\min}, r_{\max}]$.

3.6.3 The Optimization Routine. The integrated optimization method is implemented as a design optimization platform containing five modules, as shown in Fig. 6. The five modules include the computer aided design (CAD) module, the kinematic simulation, the dynamic simulation, the FEA module, and the optimization module. Among them, the CAD module is used to build the structural model of the robotic manipulators. The kinematics

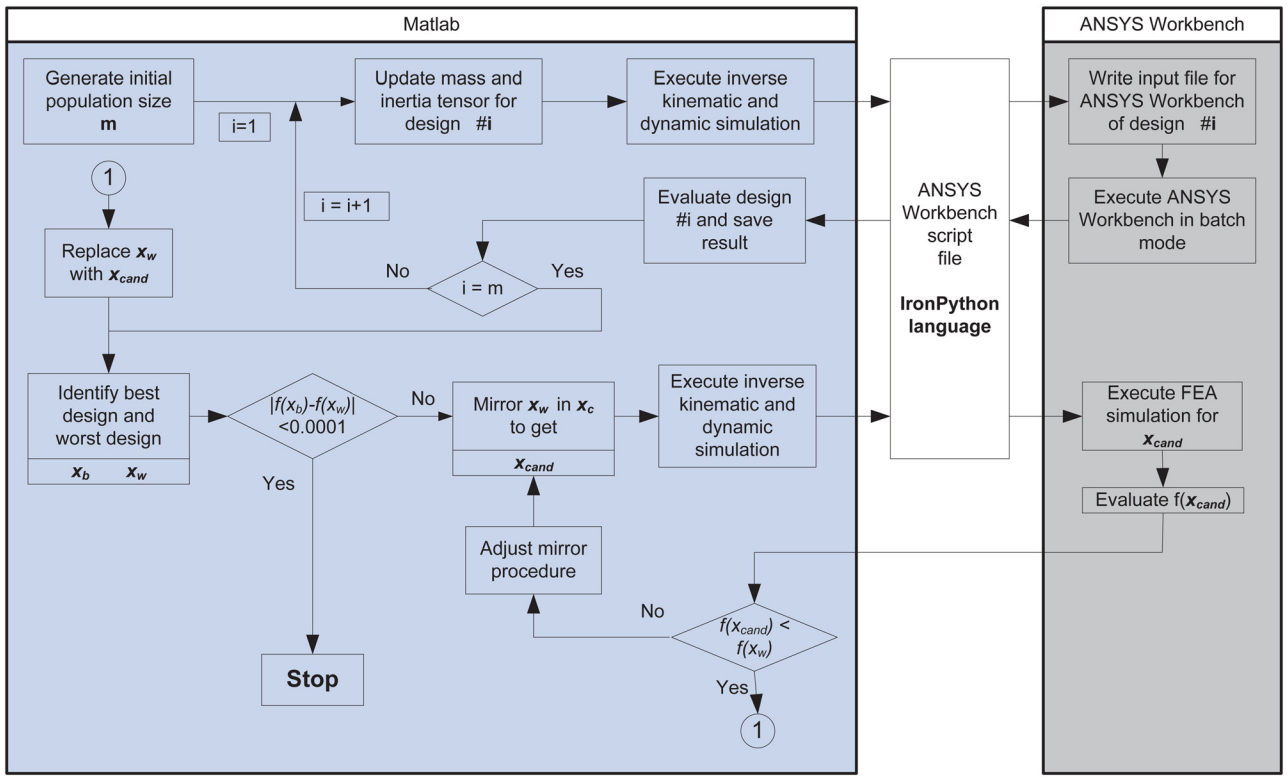

Fig. 8 Diagram of the optimization routine

Table 5 Initial and end points of end-effector trajectories

Trajectory	Initial point (mm)			End point (mm)		
	x_0	y_0	z_0	x_e	y_e	z_e
1	100	850	300	850	100	300
2	500	500	200	700	700	200
3	500	500	300	550	550	800
4	100	850	200	850	100	700

simulation module is used to conduct the kinematics analysis of the robot system. Kinematics performance, such as WS, GCI, etc., is investigated in this module. The dynamics simulation module is used to run the dynamic analysis of a multibody system. The FEA system module deals with the structural static and dynamic analysis using finite element method. The optimization module contains algorithms that are able to deal with highly nonlinear and discrete problems for running the design optimization.

In evaluating the strength and deflection, a FEA model of the robotic arm is built and simulated in ANSYS WORKBENCH™. The joint structures are imported into ANSYS WORKBENCH from CAD geometry file. The upper and lower arm links are built as parameterized model in WORKBENCH. In the FEA model, the joints are disabled, which transforms the robotic arm into a structure. The boundary conditions and loads of the robotic arm remain unchanged through the optimization iterations, as depicted in Fig. 7, where the shoulder joint of the arm is grounded. External force (payload) is applied on the gripper. The gravitational acceleration points to $-Z_0$ according to the coordinate system in Fig. 2.

The integrated optimization method was implemented in an integrated environment, where kinematic and dynamic analyses and the optimization algorithm are running in MATLAB, while

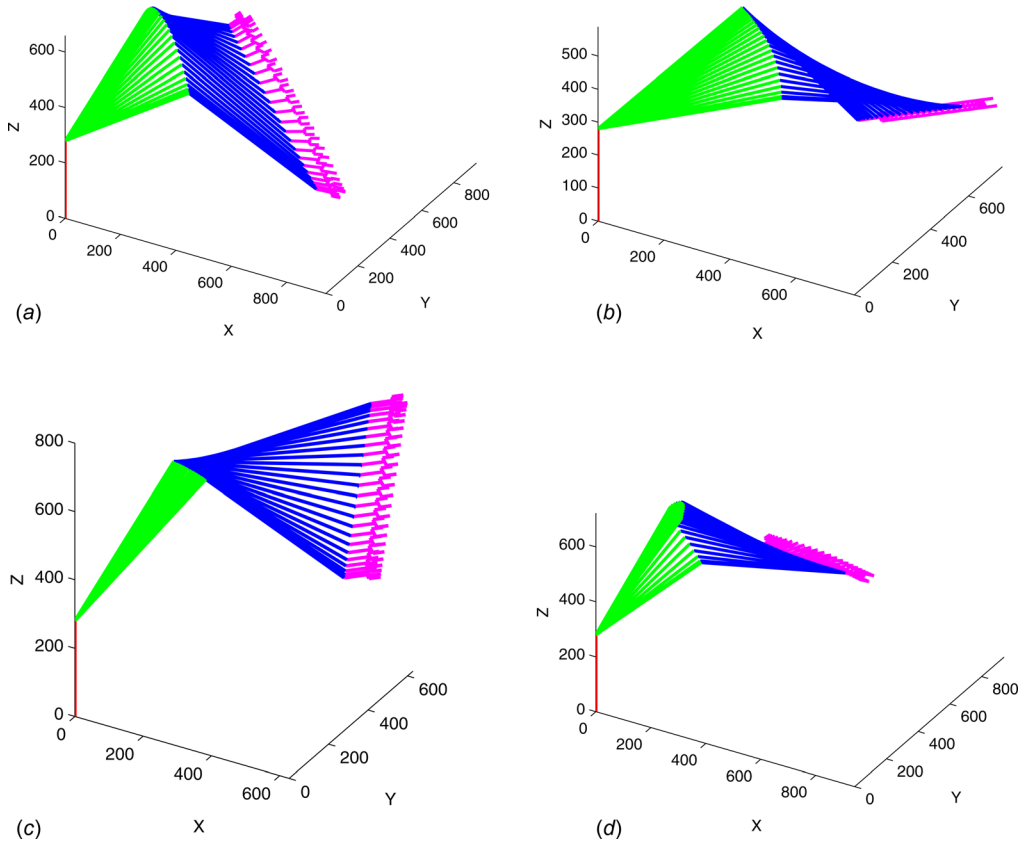

Fig. 9 Plots of the trajectories

Table 6 Results of design optimization

Joint	Initial		Case A		Case B		Case C	
	Motor	Gearbox	Motor	Gearbox	Motor	Gearbox	Motor	Gearbox
1	RE 40	CPU 17	RE 30	CPU 14	EC 32	CPU 14	RE 35	CPU 14
2	RE 35	CPU 17	RE 25	CPU 14	RE 25	CPU 14	RE 25	CPU 14
3	RE 35	CPU 17	RE 30	CPU 14	RE 30	CPU 14	RE 35	CPU 14
4	RE 35	Gearhead	RE 25	Gearhead	RE 25	Gearhead	RE 25	Gearhead
5	RE 35	CPU 17	RE 25	CPU 14	RE 25	CPU 14	RE 25	CPU 14
Ratio	$r=0.5$		$r=0.6$		$r=0.6$		$r=0.5$	
Weight	16.7 (kg)		8.3 (kg)		9.92 (kg)		9.98 (kg)	

Case A: Optimization with the new method.
Case B: Optimization of drive-train with kinematic constraints.
Case C: Optimization of drive-train only [6].

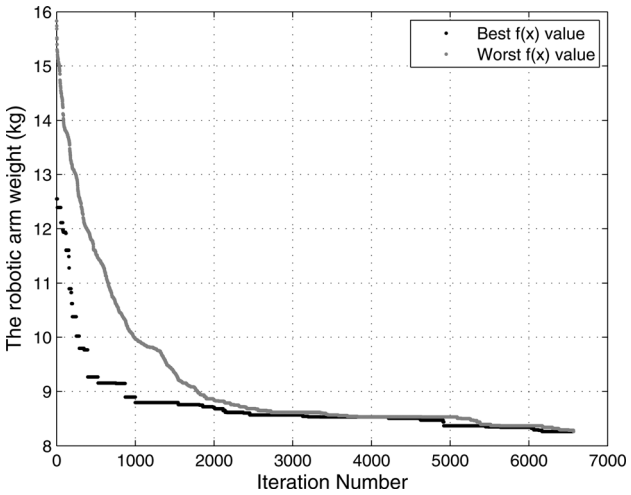

Fig. 10 Convergence of the weight of the robotic arm

strength analysis is executed through ANSYS WORKBENCH. Interface was developed to allow data exchange between MATLAB and ANSYS. The flow diagram of the optimization routine is shown in Fig. 8.

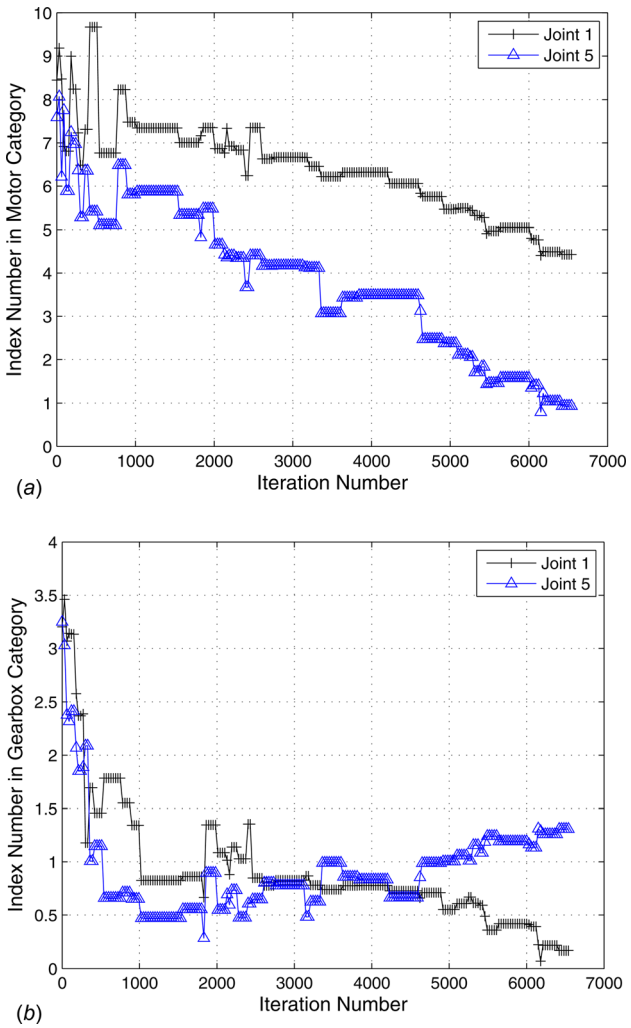

Fig. 11 Convergence plots for the design variables of motors and gearboxes

The FEA in ANSYS WORKBENCH is very computationally expensive. It takes 5 min for a single simulation of the static analysis. To improve the efficiency, FEA simulations were conducted in batch mode for the discrete structural dimensions, and the results consisting of maximum stress, deformation, and mass are stored in a database file. In each iteration of the optimization, the program will load the results from the database for the integrated optimization instead of running FEA simulation. It takes about 4 h to build the database. Adopting this approach avoid the repeated calculated in the strength analysis, thus leading to the computational time reduced from more than 10 days for one case to 10 min only.

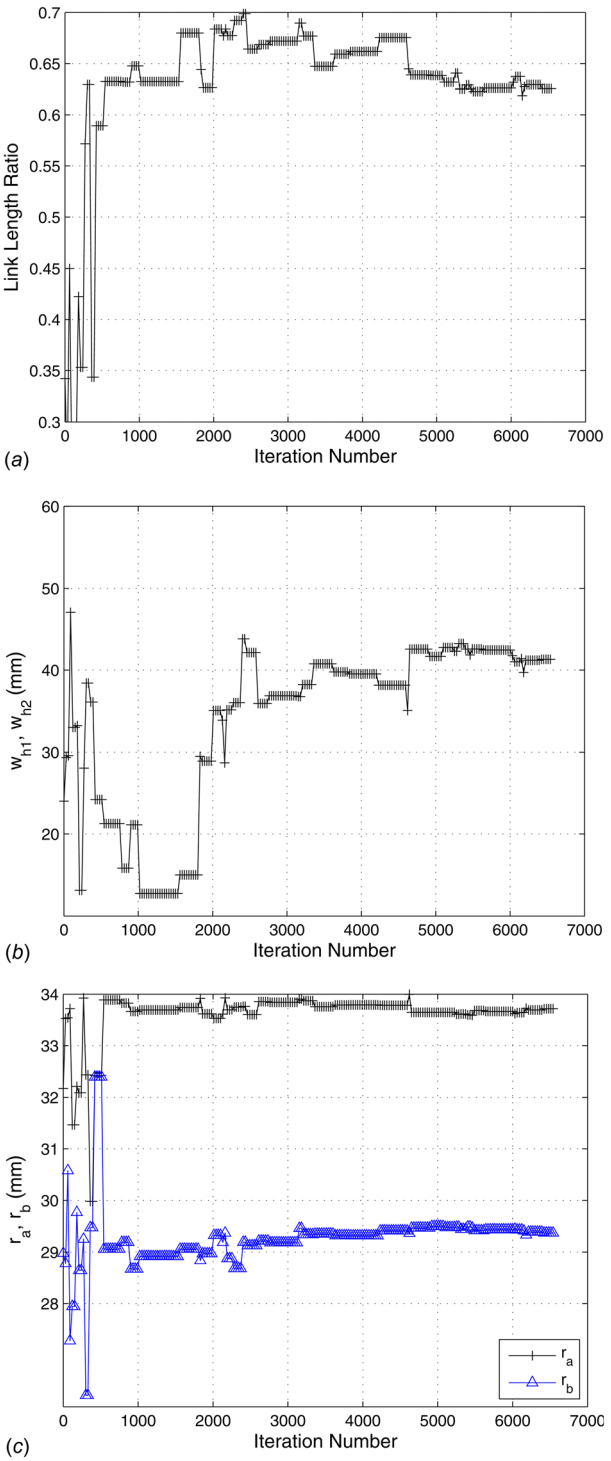

Fig. 12 Convergence of dimensional variables. (*a*) Link length ratio, (*b*) w_{h1} and w_{h2}, and (*c*) r_a and r_b.

Table 7 Optimal structural dimensions (mm)

	l_1	r_a	r_b	w_{h1}	w_{h2}
Original	500	31	27	20	20
Optimized	600	34	29	40	40

4 The Arm Design Optimization

The design of the 5 dof lightweight arm is included to demonstrate the developed method. Prior to design optimizations, trajectories are defined for kinematic and dynamic analysis.

4.1 Arm Trajectories. To simplify the trajectory definition, straight-line motion is selected for the robotic arm. A straight line motion, starting from an initial point $\mathbf{p}_0 = (x_0, y_0, z_0)^{\mathrm{T}}$ at $t = 0$ to an ending point $\mathbf{p}_e = (x_e, y_e, z_e)^{\mathrm{T}}$ at time $t = T$, can be expressed as

$$\mathbf{p} - \mathbf{p}_0 = u_p(\mathbf{p}_e - \mathbf{p}_0), \quad u_p \in [0, 1] \tag{19}$$

where the parameter u_p controls the movement of the end-effector. A trajectory with $\mathcal{C}^2$-continuity can be planned as

$$u_p(t) = p_0 + p_1 t + p_2 t^2 + p_3 t^3 \tag{20}$$

where p_0, p_1, p_2, and p_3 are constant coefficients. Assuming the velocities at the initial and ending point are $\dot{\mathbf{p}}_0 = (\dot{x}_0, \dot{y}_0, \dot{z}_0)^{\mathrm{T}}$ and $\dot{\mathbf{p}}_e = (\dot{x}_e, \dot{y}_e, \dot{z}_e)^{\mathrm{T}}$, the four constant coefficients can be solved.

In this work, we use a group of four trajectories to conduct kinematics and dynamics simulation on the robotic arm, with the coordinates of the initial and end points of the trajectories listed in Table 5. Among them, the end-effector moves horizontally following trajectory 1, while moves vertically with trajectory 2. Trajectories 3 and 4 are paths of different inclination. The robotic arm starts to move from rest and stops in five seconds. The Euler angles for the end-effector are given as $[0, \cos(t/20), 0]$, which implies the end-effector remains horizontal during the motion. The trajectories are plotted in Fig. 9.

In each iteration of the optimization, the kinematics and dynamics are analyzed with respect to the four trajectories. The maximum torques of each joint are used to select motors and gearboxes for the drive train. Depending on the applications, the group of trajectories can be extended to contain more trajectories for more detailed evaluations of torque requirements of the robotic arm.

4.2 Material Strength Limits. The payload is defined as a point mass of 5 kg. In the FEA, the design payload is multiplied by a safety factor, i.e., $F_{\mathrm{A}} = 100$ (N). The structure parts of this robot in this work are made of aluminum, so the yield strength $S_{\mathrm{y}} = 280$ MPa. The deflection limit at the end-effector is set to $D_{\mathrm{lim}} = 5$ mm.

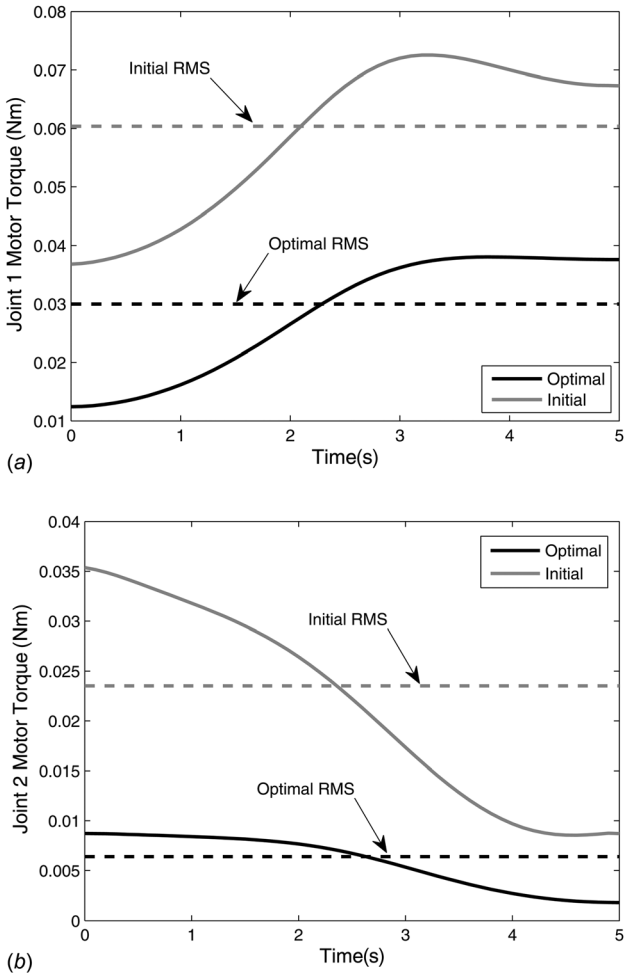

Fig. 14 Motor torques for initial and optimal drive-train combinations. (*a*) Joint 1 and (*b*) Joint 2.

4.3 Candidate Components. Nine candidate motors from the Maxon Motor catalogue are considered. They are listed in a database ascendingly with respect to the mass of motor, as shown in Table 8 of the Appendix. The gearboxes used in the robotic arm are selected from Harmonic Drive CPU units, as listed in Table 9 of the Appendix. For the Harmonic Drive gearboxes, the

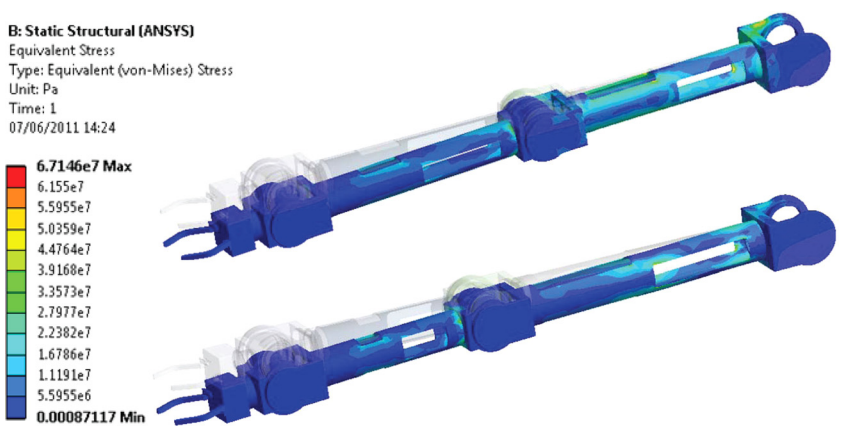

Fig. 13 von-Mises element stress in the original (top) and optimized (bottom) robotic arm

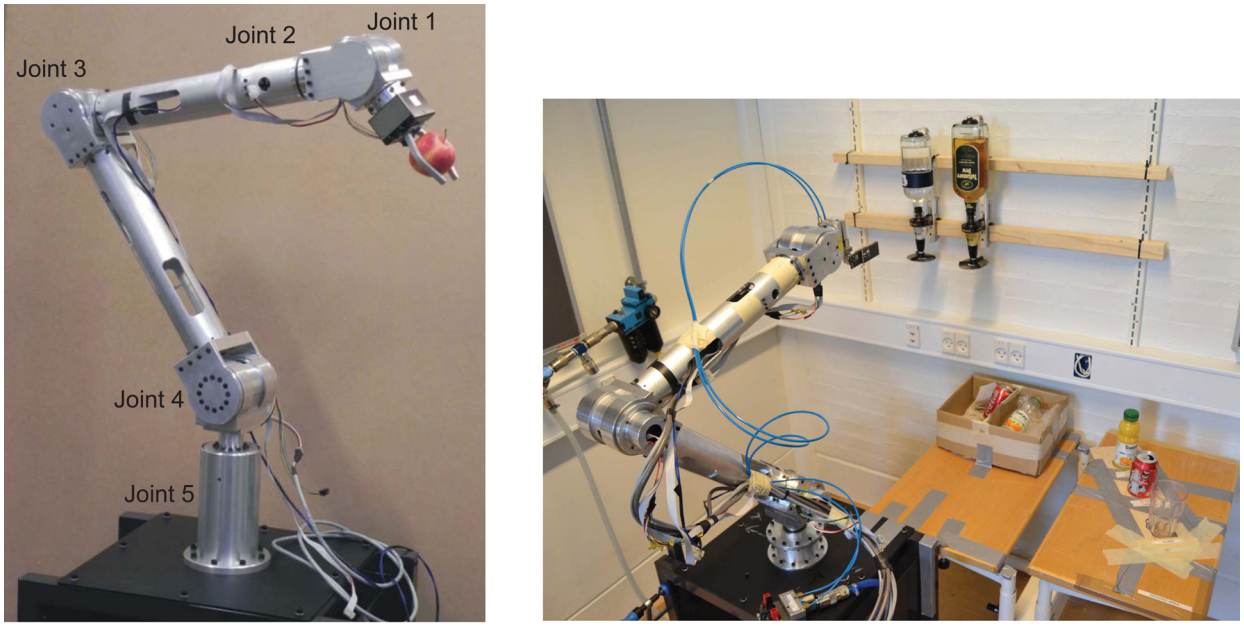

(*a*) (*b*)

Fig. 15 Prototypes of the robot arm. (*a*) First prototype and (*b*) second prototype for drink serving (demo video in Ref. [25]).

efficiency is a function of operation speed. In this work, the gear efficiency is set to 0.85 for all gearboxes, which is an average value from product catalog.

The gear ratios of all joints set to $\rho = \{200, 200, 200, 51, 100\}$, orderly from joint 1 to joint 5. Note there are two-stage gearboxes in joints 1, 2, and 3, consisting of a planetary gearhead and a Harmonic Drive unit. For simplicity, only the mass of the Harmonic Drive gearbox is parameterized, while the mass of the planetary gearhead is set to constant. The Harmonic Drive CPU unit is adopted in all joints except joint 4, due to the joint structure consideration. A planetary gearhead is used in joint 4, so $u_{g,4} = 0$.

4.4 Optimization Results. Optimized designs of the structure and drive-train for the robotic arm are listed in Table 6. As shown in the optimization results of case A, the optimized weight of the robotic arm is 8.3 kg, a mass reduction to 50% of the initial design being achieved.

The convergence of the objective function is depicted in Fig. 10, both the best (black dot) and worst values (gray dot) from the complex algorithm are shown. The solution to the optimal result is achieved at 6500 iterations with 150 population sizes. In this work, the tolerance of convergence is equal to 0.0001.

Figure 11(*a*) illustrates the convergence of motor design variables. Only the convergence plots for joints 1 and 5 are displayed for clarity. The convergence of gearbox design variables is depicted in Fig. 11(*b*). The round function is used to treat the design variables, such that they can be used to select components from the database. Comparing the convergence rate for the motor and gearbox design variables, the gearbox design variables converging rate towards the optimal results is faster than the motor design variables. This phenomenon is caused by that the mass difference among Harmonic Drive units is larger than among motors.

The convergence of the link length ratio is shown in Fig. 12(*a*). The link length ratio is converged to $r = 0.6$. The design variable of link length ratio is treated by the round function defined in Sec. 3.6.2. The limit of kinematic performance GCI is set to $C_{\min} = 0.02$, a limit that can be satisfied by a robotic arm with link ratios between $r = 0.2$–0.8. Coincidently, this ratio is close to that of the industrial robots [24].

The lengths of the upper arm link l_{s1} and lower arm link l_{s2} are obtained from the link length ratio r. The optimized structural dimensions of the robotic arm are shown in Table 7. The convergence plots of the inner radius and widths of the opening slots are depicted in Fig. 12. Note that to reduce calculation, w_{h1} is made identical to w_{h2} in this work. By using the structural dimensions in Table 7, FEA is conducted separately for the original and optimized robotic arm designs, with the von-Mises element stress being depicted in Fig. 13.

The variations of motor torques of joints 1 and 2 for the initial and the optimal designs of case A are shown in Fig. 14. The simulation is based on trajectory 1 in Table 5. The torques of the optimal design are depicted in black color, and those of the initial design are in gray. The RMS value of each torque is depicted with dashed line. It is seen that the optimal design has a reduction of 51% RMS torque for joint 1, and a reduction of 72% RMS torque for joint 2.

The optimization results were compared with the results from a previous method [6]. Two additional cases, namely, for optimization of drive-train with kinematic constraints and case C for

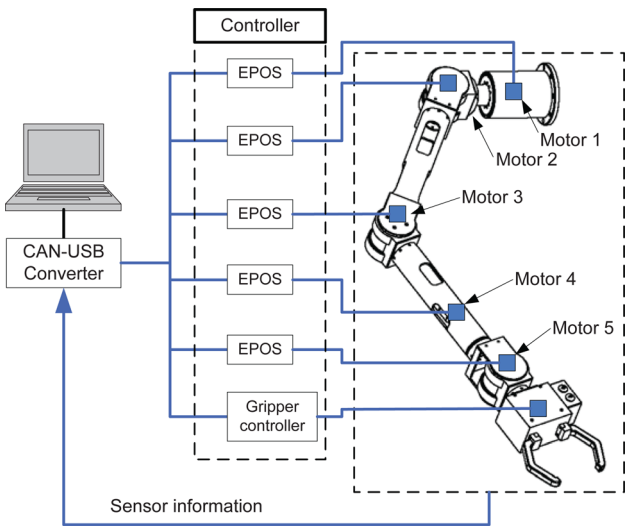

Fig. 16 Control system of the robotic arm

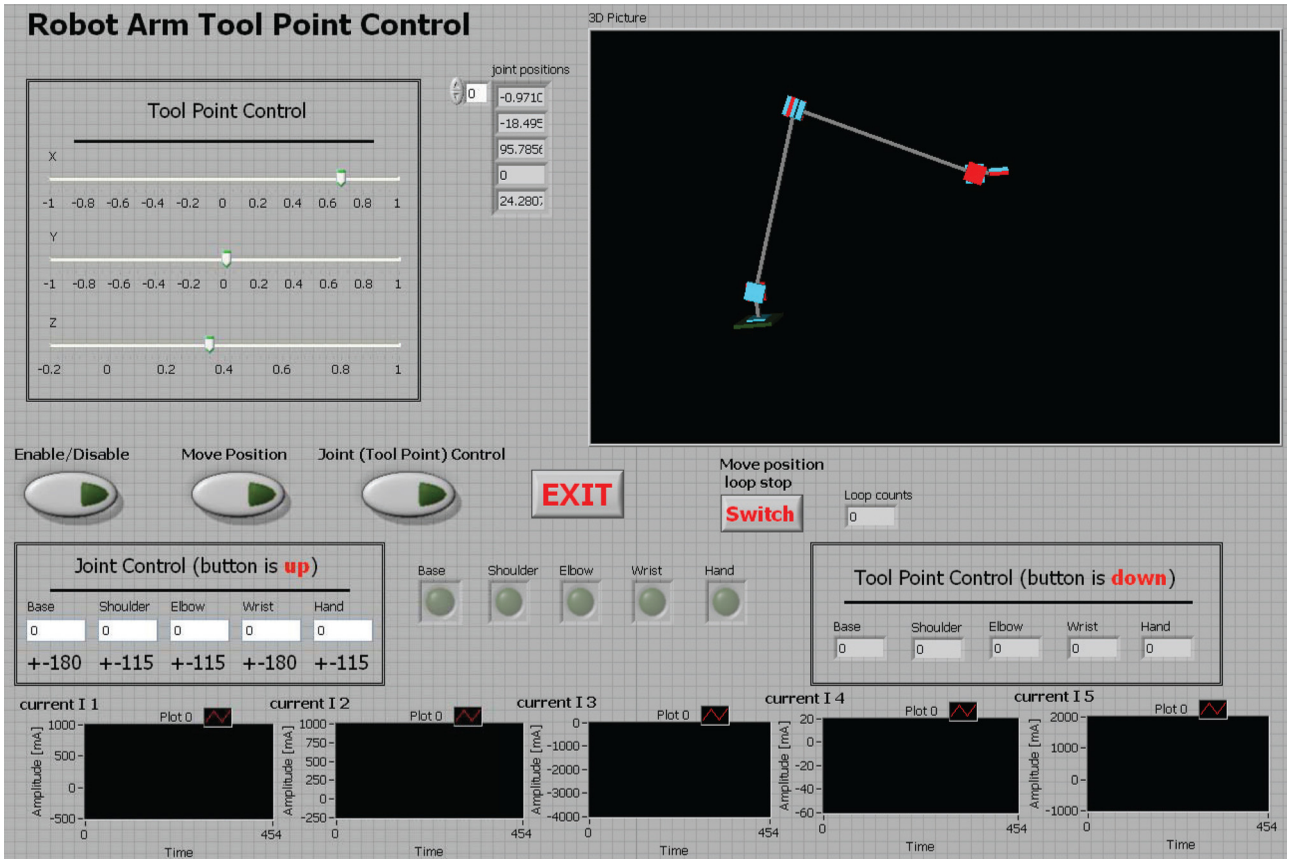

Fig. 17 User interface of the robotic arm control

optimization of drive-train only are considered for comparison. The optimization results are listed in Table 6. It is seen that the weight change of the robot is not significant in the two optimized cases without strength constraints, no matter the kinematic constraints are included or not. A major mass reduction is achieved with the optimization under the constraint of strength, which reduces the mass of the upper and lower arm links by 1.7 kg. The comparison reveals that the new method can contribute to reduce further the robot mass without degrading the performance of the robot.

5 Robot Prototyping

Prototypes of the robotic arm were built, as shown in Fig. 15. The components of drive-train in the prototype were selected and scaled based on the optimization results shown in Table 6. In total, two prototypes were built. The second one was constructed by modifying the first one, with a redesign base joint for improvement of joint stiffness. Moreover, a new gripper driven pneumatically was used for the reason of compatible drivers.

5.1 System Integration. The arm joints are driven by electrical motors, chosen among Maxon DC motors. The five motors have different power ratings, depending on the load in the joints; the used models are 60 W, 70 W, and 90 W. For precise measurement of the angle during operation, an encoder is mounted on each motor. These are of the type Maxon Encoder MR, Type L, 1024 CPT, 3 Channels, and provide a relative measurement of the angle with 1000 pulses each turn.

Each motor is connected to an amplifier, namely, the Maxon EPOS2 24/5 amplifier, which has a built-in PID-controller, A/D converter, digital I/O, and CAN-bus. The built-in PID-controller enables speed and position control by use of the encoders mounted on the motors. Additionally, the EPOS amplifier also enables current control, i.e., torque control of the motor.

CANopen (Controller Area Network) bus is adopted for the communications between motors and controllers, as shown in Fig. 16. The interface to the EPOS amplifier adopts the CANopen protocol, which ensures that the measurements can be fetched and the control of the motors can be achieved digitally via the CANopen bus, i.e., the entire motor setup is noise immune. CAN runs a two-wire differential serial communication protocol, the CANopen protocol, for real-time control. CANopen protocol uses the CAN Physical Layer as defined by the CAN in Automation (CiA) standard "DS-301 Version 4.02." The communications between CANopen bus and the PC are accomplished by a CAN–USB interface.

5.2 Motion Control Program. The control program is developed in NI.LabView through utilizing toolbox of EPOS controller, as the control panel shown in Fig. 17. A tool point control scheme is developed for the arm. The arm is controlled in the working space through manipulating the Cartesian coordinates of the gripper.

The lightweight robot has been tested as a bartender serving drinks, as shown in Fig. 15(*b*). Following predefined trajectory, the robot was able to deliver a drink successfully (see video in Ref. [25]). PID parameters were tuned for smooth movements.

6 Discussion and Conclusions

A lightweight robotic arm was designed and developed utilizing the proposed design method, in which design criteria of lightweight and compliance are met by the integrated design optimization. Selections of structural dimensions, motors, and gearboxes were formulated as a discrete optimization problem, which was solved by a nongradient optimization method. GCI was taken as a constraint on kinematics performance of the robot. The results show that the method can achieve an optimal design with

minimum mass, while satisfying the constraints on kinematics, drive-train, and structural strength.

A new approach of integrating strength analysis together with the kinematic and dynamic analysis is developed in the work. The inclusion of the robot structural strength in the optimization benefits the robot design in several aspects. First, the mass can be effectively reduced by applying the static strength constraint, as did in this work. Second, this approach can also address the fatigue limit, a major concern in robot design, by either specifying a minimum stress or conducting fatigue simulation in FEA module.

The proposed approach provides a systemic design optimization method for robots. For a draft robot design with given joint configurations, the approach can be used to select drive-train components and structural dimensions for lightweight purpose. The consideration of structural strength in the integrated design optimization brings in new research problems for future research. For example, a stiffness model can also be considered to facilitate the stiffness evaluation for all configurations [26]. In the current design, the topology of the arm links is fixed to the opening slots. Integrating the topology optimization into the integrated design could also be considered [27]. Other future work may include the generalization of this method for different objectives and also the integration of robot control into the optimization. While arm morphology is not considered in the optimization, it remains an open problem for future research.

Acknowledgment

The project is sponsored by Aalborg University and Det Obelske Familiefond (DOF). The authors are very grateful to Professor Michael R. Hansen from University of Agder, Norway, for his helpful discussion on many technical problems. Students Martin Bang Nielsen, Simon Christensen, Soeren Elton Mark, and Rick Peters built the second prototype.

Appendix

Table 8 Candidate motor data from Maxon Motor [28]

Index no.	Maxon Motor	T_m (Nm)	T_m^{max} (Nm)	N_m^{max} (rpm)	J_m ($g\,cm^2$)	m_m (kg)
1	RE 25	0.0284	0.28	14,000	10.5	0.13
2	RE 26	0.0321	0.227	14,000	12.1	0.15
3	EC-i 40	0.0667	1.81	15,000	24.2	0.21
4	RE 30	0.0882	1.02	12,000	34.5	0.238
5	EC 32	0.0426	0.353	25,000	20	0.27
6	RE 35	0.0965	0.967	12,000	67.4	0.34
7	RE 36	0.0795	0.785	12,000	67.2	0.35
8	EC 40	0.127	0.94	18,000	85	0.39
9	RE 40	0.184	2.5	12,000	138	0.48

Table 9 Candidate gearbox data from Harmonic Drive [29]

Index no.	Unit size	T_g (Nm)	T_g^{max} (Nm)	N_g^{max} (rpm)	J_g ($kg\,m^2$)	m_g (kg)
1	14	11	54	8500	0.033×10^{-4}	0.54
2	17	39	110	7300	0.079×10^{-4}	0.79
3	20	49	147	6500	0.193×10^{-4}	1.3
4	25	108	284	5600	0.413×10^{-4}	1.95

References

[1] Albu-Schäffer, A., Haddadin, S., Ott, C., Stemmer, A., Wimböck, T., and Hirzinger, G., 2007, "The DLR Lightweight Robot: Design and Control Concepts for Robots in Human Environments," Ind. Rob., **34**(5), pp. 376–385.
[2] Chedmail, P., and Gautier, M., 1990, "Optimum Choice of Robot Actuators," ASME J. Manuf. Sci. Eng., **112**(4), pp. 361–367.
[3] Sardellitti, I., Park, J., Shin, D., and Khatib, O., 2007, "Air Muscle Controller Design in the Distributed Macro-Mini (DM^2) Actuation Approach," Proceedings of the IEEE/RSJ International Conference on Intelligent Robots and Systems (IROS 2007), San Diego, CA, Oct. 29–Nov. 2, pp. 1822–1827.
[4] Pettersson, M., and Ölvander, J., 2009, "Drive Train Optimization for Industrial Robots," IEEE Trans. Rob., **25**(6), pp. 1419–1423.
[5] Elmqvist, H., Olsson, H., Mattsson, S. E., and Brück, D., 2005, "Optimization for Design and Parameter Estimation," International Modelica Conference, Hamburg, Germany, Mar. 7–8, pp. 255–266.
[6] Zhou, L., Bai, S., and Hansen, M. R., 2011, "Design Optimization on the Drive Train of a Light-Weight Robotic Arm," Mechatronics, **21**(3), pp. 560–569.
[7] Roy, J., and Whitcomb, L. L., 2004, "Comparative Structural Analysis of 2-DOF Semi-Direct-Drive Linkages for Robot Arms," IEEE/ASME Trans. Mech., **4**(1), pp. 82–86.
[8] Pil, A., and Asada, H., 1995, "Rapid Recursive Structure Redesign for Improved Dynamics of a Single Link Robot," ASME J. Dyn. Syst. Meas. Control, **117**(4), pp. 520–526.
[9] Bai, S., and Zhou, L., 2011, "Design Optimization of a 5 Light-Weight Robotic Arm Under Structural Constraints," 24th Nordic Seminar on Computational Mechanics, Helsinki, Finland, Nov. 3–4, pp. 119–123.
[10] Zhu, Y., Qiu, J., and Tani, J., 2001, "Simultaneous Optimization of a Two-Link Flexible Robot Arm," J. Rob. Syst., **18**(1), pp. 29–38.
[11] Rout, B. K., and Mittal, R. K., 2010, "Optimal Design of Manipulator Parameter Using Evolutionary Optimization Techniques," Robotica, **28**(3), pp. 381–395.
[12] Shiller, Z., and Sundar, S., 1991, "Design of Robotic Manipulators for Optimal Dynamic Performance," IEEE International Conference on Robotics and Automation, Sacramento, CA, Apr. 9–11, pp. 344–349.
[13] Zhou, L., Bai, S., and Hansen, M. R., 2012, "Integrated Dimensional and Drive-Train Design Optimization of a Light-Weight Anthropomorphic Arm," Rob. Auton. Syst., **60**(1), pp. 113–122.
[14] Denavit, J., and Hartenberg, R. S., 1955, "A Kinematic Notation for Lower Pair Mechanisms Based on Matrices," ASME J. Appl. Mech., **77**, pp. 215–221.
[15] Fang, Y., and Tsai, L. W., 2003, "Inverse Velocity and Singularity Analysis of Low-DOF Serial Manipulators," J. Field Rob., **20**(4), pp. 177–188.
[16] Yoshikawa, T., 1985, "Manipulability of Robotic Mechanisms," Int. J. Rob. Res., **4**(2), pp. 3–9.
[17] Gosselin, C., and Angeles, J., 1991, "A Global Performance Index for the Kinematic Optimization of Robotic Manipulators," ASME J. Mech. Des., **113**(3), pp. 220–226.
[18] Bai, S., 2010, "Optimum Design of Spherical Parallel Manipulators for a Prescribed Workspace," Mech. Mach. Theory, **45**(2), pp. 200–211.
[19] Harmonic Drive, "Engineering Data for Harmonic Drive Gears," Harmonic Drive AG, Limburg/Lahn, Germany, www.harmonicdrive.de/cms/upload/pdf/en/cpu_h7.pdf
[20] Norten, R. L., 2010, *Machine Design: An Integrated Approach*, 4th ed., Prentice-Hall, Englewood Cliffs, NJ.
[21] Antony, G. G., "Rating and Sizing of Precision Low Backlash Planetary Gearboxes for Automation Motion Control and Robotics Applications," Neugart USA Corp., Bethel Park, PA, www.neugartusa.com/Service/faq/Gear_Rating.pdf
[22] Box, M. J., 1965, "A New Method of Constrained Optimization and a Comparison With Other Methods," Comput. J., **8**(1), pp. 42–52.
[23] Guin, J. A., 1968, "Modification of the Complex Method of Constrained Optimization," Comput. J., **10**(4), pp. 416–417.
[24] Kucuk, S., and Bingul, Z., 2006, "Comparative Study of Performance Indices for Fundamental Robot Manipulators," Rob. Auton. Syst., **54**(7), pp. 567–573.
[25] Nielsen, M. B., Christensen, S., Mark, S. E., and Peters, R., 2012, "Light-Weight Robotic Arm Serving Drink," Aalborg University, Aalborg, Denmark, https://www.youtube.com/watch?v=yLPBrK_sjjI&feature =g-all-u
[26] Kucuk, S., 2013, "Energy Minimization for 3-RRR Fully Planar Parallel Manipulator Using Particle Swarm Optimization," Mech. Mach. Theory, **62**, pp. 129–149.
[27] Sigmund, O., 1997, "On the Design of Compliant Mechanisms Using Topology Optimization," Mech. Struct. Mach., **25**, pp. 493–524.
[28] Maxon Motor, Products Catalogue 10/11, Maxon Motor, Sachseln, Switzerland, www.maxonmotor.ch/e-paper/blaetterkatalog/pdf/complete.pdf
[29] Harmonic Drive, 2014, Harmonic Drive Technical Data, Harmonic Drive AG, Limburg/Lahn, Germany, www.harmonicdrive.de/cms/upload/German/B_Produkte/B_Units/kompl_Produktkapitel_CPU_D-E.pdf